

## EFFECT OF PARTICLE SIZE OF $\text{BaFe}_{12}\text{O}_{19}$ ON THE MICROWAVE ABSORPTION CHARACTERISTICS IN X-BAND

Abhishek Kumar<sup>1</sup>, Vijaya Agarwala<sup>1</sup>,  
and Dharmendra Singh<sup>2, \*</sup>

<sup>1</sup>Metallurgical & Materials Engineering Department, Indian Institute of Technology Roorkee, Roorkee, India

<sup>2</sup>Electronics & Computer Engineering Department, Indian Institute of Technology Roorkee, Roorkee, India

**Abstract**—Present work deals with the microwave absorption characteristics of  $\text{BaFe}_{12}\text{O}_{19}$  of interest as radar absorbing material (RAM). There are very few reported works available where particle size has been critically analyzed for absorbing characteristics at microwave frequencies, therefore, in this paper microwave absorption properties of the  $\text{BaFe}_{12}\text{O}_{19}$  with different particle sizes were investigated. The results showed that the particle size had significant influence on the dielectric and absorption properties of the composites in the 8.2–12.4 GHz frequency range.  $\text{BaFe}_{12}\text{O}_{19}$  powder of different particle sizes were synthesized by varying the annealing time and it was observed that the real part of permittivity of the composite increases from 5.18 (average value) to 7.50 (average value) and imaginary part increases from an average value of 0.20 to an average value of 2.33, whereas the real part of permeability increases from 0.95 (average value) to 1.11 (average value) and imaginary part of permeability was measured in the range of 0.02 to 0.07. These changes in permittivity and permeability affects microwave absorption application. It is observed that the maximum bandwidth for average particle size of 240 nm is 3.02 GHz and with the increase in average particle size, microwave absorption properties increased.

---

*Received 16 January 2013, Accepted 16 February 2013, Scheduled 8 March 2013*

\* Corresponding author: Dharmendra Singh (dharmfec@gmail.com).

## 1. INTRODUCTION

Recently, electromagnetic interference (EMI) problems have seriously increased with the fast technological developments and extensive use of electromagnetic (EM) waves in wireless communication at higher frequencies [1]. These EMI problems have been attracting more attention over military and civilian spheres due to the extensive growth in electric components [2]. All types of electrical components are subjected to the EM interference induced by electric and magnetic fields, therefore, microwave absorbers are the focus of extensive study. Conventional spinel type ferrites do not function well in the GHz range due to a drop in the complex permeability ( $\mu_r$ ) as given by Snoek's limit [3]. Metallic magnetic materials show high permeability, but they have to be insulated to prevent an eddy current due to a drop in the complex permeability ( $\mu_r$ ) in the GHz range [4]. Electric and magnetic energy storage capabilities of a material are represented by real parts of complex permittivity ( $\epsilon'$ ) and permeability ( $\mu'$ ). The imaginary parts ( $\epsilon''$ ,  $\mu''$ ) represent the loss of electric and magnetic energy. M-type hexagonal ferrites in comparison to spinel ferrites and metallic magnetic materials have higher saturation magnetization, greater coercivity, excellent thermal and chemical stability, corrosion resistance and adjustable anisotropy, therefore they can be used as microwave absorbers in the GHz frequency range. Being a hard magnetic material, Barium hexaferrite has been a subject of continuous interest for several decades due to its applicability in electronic components, magnetic memories and recording media. It is also used as a dielectric or magnetic filler in the electromagnetic filler attenuation materials (EAM) [5].

There are many methods of producing ferrites, which include classical ceramic method, the dry milling method, the co-precipitation method, the hydrothermal reaction and the sol-gel auto-combustion method etc.. Every method has its own advantages and disadvantages. For example, the classical ceramic method requires high calcination temperature of the order of 1300–1400°C for reaction to take place, which often results in the formation of coarse aggregate and the resulting particle size of the powder is about 1  $\mu$ m and some of the components are easily vaporized at such a high temperature [6]. The conventional dry milling method has disadvantages such as time consuming and introduces impurities into material compositions, which causes the lattice to strain in crystal structure and irregularity of particle shape. However, by using sol-gel autocombustion method, the disadvantages of introduction of impurities, requirement of milling time and high calcination temperature are eliminated. The sol-gel

autocombustion follows sol-to-gel (S-G) conversion and then after annealing, gel-to-crystalline (G-N) conversion takes place. Still, it is challenging to develop a material with less complexity and considerable absorbing capabilities. It is observed that material composition and particle morphology play a major role in absorption behavior.  $\text{BaFe}_{12}\text{O}_{19}$  is commonly used as a microwave absorbing material and is continuously of interest for the last many decades. Several researchers have developed different compositions of  $\text{BaFe}_{12}\text{O}_{19}$  substituted by different metal elements like Al, Co, Cr, Mg, Ni, Mn and Ti for microwave absorption [2, 9–13], but the effect of particle size is still under research and very less attention has been given to observe the effect of particle size on absorption at microwave frequencies. The particle morphology and particle size are influenced by heat treatment [7, 8]. It has been observed that the average particle size grows exponentially with the heating temperature and linearly with the heating time period [8].

Therefore, in this paper an attempt has been made to study the effect of M-type Barium hexaferrite ( $\text{BaFe}_{12}\text{O}_{19}$ ) particle size on microwave absorption at X-band (8.2–12.4 GHz) where sol-gel autocombustion method was used for synthesis and ferrite particles were grown in size by increasing the annealing time. The effect of particle size on complex permittivity, complex permeability and microwave absorption has been studied. This paper is organized as follows. Section 2 briefly describes synthesis of ferrite and characterization techniques used. The experimental results are discussed in Section 3, which includes thermal analysis, phase analysis, morphology, particle size analysis and EM characterization through waveguide measurements. Finally conclusion is discussed in Section 4.

## 2. EXPERIMENTAL PROCEDURE

### 2.1. Synthesis of Ferrite

Analytical grade  $\text{Ba}(\text{NO}_3)_2$ ,  $\text{Fe}(\text{NO}_3)_3 \cdot 9\text{H}_2\text{O}$ , citric acid ( $\text{C}_6\text{H}_8\text{O}_7 \cdot \text{H}_2\text{O}$ ) and  $\text{NH}_4\text{OH}$  were used as the starting materials. Stoichiometric amounts of  $\text{Fe}(\text{NO}_3)_3 \cdot 9\text{H}_2\text{O}$  and  $\text{Ba}(\text{NO}_3)_2$  were dissolved in double distilled (Millipore) water and then citric acid ( $\text{C}_6\text{H}_8\text{O}_7 \cdot \text{H}_2\text{O}$ ) was added into the solution with the ratio of citric acid to metal ion 1.5. The pH of the solutions was adjusted to a value of 9 using ammonium solution. Subsequently, after evaporation at  $80^\circ\text{C}$  and continuous stirring, the solution was transformed into a brown wet gel and then this freshly obtained brown gel was allowed for auto-combustion. After auto-combustion, the combustion product powders were annealed at  $1100^\circ\text{C}$  in air atmosphere to form the desired phase and the particle

size was grown by increasing the annealing time. For the same, the 'as-synthesized' powder (represented as  $P_0$ ) was annealed at 1100°C for different holding times of 2, 4 and 8 hours to change the particle size and represented as  $P_1$ ,  $P_2$  and  $P_3$  respectively which are shown in Table 1.

## 2.2. Characterization Studies

Thermal study of barium hexaferrites was carried out in air by differential scanning calorimetry (Perkin Elmer, Pyris Diamond). Phase identification of annealed samples was done by XRD using Bruker AXS D8 diffractometer with Cu- $K_\alpha$  radiation. The crystallite size of the powders were measured by X-ray line broadening technique employing Scherrer's formula. The surface morphology of the annealed

**Table 1.** Unit cell parameter of the Ba-hexaferrites.

Sample Code		$P_0$	$P_1$		$P_2$		$P_3$	
XRD Peak		Highest	Highest	IInd Highest	Highest	IInd Highest	Highest	IInd Highest
$2\theta^\circ$	Standard	35.707	34.268	32.451	34.268	32.451	34.268	32.451
	Observed	35.697	34.396	32.477	34.228	32.290	34.185	32.240
FWHM ( $^\circ$ )		0.293	0.167	0.174	0.161	0.170	0.16	0.166
$I/I_{\max}$		100	100	85.9	100	83.9	100	88.1
$I_{35.697}/I_{\max}$		-	4.85		7.00		6.78	
Miller Indices		-	(114)	(017)	(114)	(017)	(114)	(017)
Lattice 'a' ( $\text{\AA}$ )		-	5.840		5.861		5.862	
Lattice 'c' ( $\text{\AA}$ )		-	23.628		23.723		23.769	
$c/a$		-	4.045		4.047		4.054	
Volume of unit cell ( $\text{\AA}^3$ )		-	698.11		705.9		707.25	
Crystallite size (nm)		35.5	72	66.1	76.1	68.4	76.9	70.9
Particle Size (nm) $\pm$ STDV (nm)		37	125 $\pm$ 70		156 $\pm$ 108		240 $\pm$ 134	

powders were studied by FE-SEM using QUANTA FEG 200 FEI and transmission electron microscope, TEM (Philips, EM 400; TECHNAI 20G2-S-TWIN). To study the microwave dielectric properties, all the samples (80 wt.%) were mixed with epoxy resin and 2% hardener. The ferrite-epoxy composites thus obtained were cast into a rectangular pellet of thickness 2.2 mm and cured at 60°C for 2 h. The composites thus prepared were polished to exactly fit into the measuring waveguide (WR-90). The complex permittivity and permeability measurements were carried out on Network Analyzer (Agilent N5222 PNA series) using 'Poly Ref/Tran'  $\mu$  &  $\epsilon$  model of material measurement software 85071 in the frequency range of 8.2–12.4 GHz at room temperature. The values of Reflection loss (RL) were calculated from the complex permittivity and permeability at given frequency and absorber thickness using the following equations [3, 9, 10, 15–17]:

$$Z_{in} = Z_o(\mu_r/\epsilon_r)^{1/2} \tanh \left\{ j(2\pi f d/c)(\mu_r \epsilon_r)^{1/2} \right\}$$

$$RL = -20 \log |(Z_{in} - Z_o)/(Z_{in} + Z_o)|$$

where,  $f$  is measurement frequency (in our case 8.2–12.4 GHz),  $d$  the thickness of absorber,  $c$  the velocity of light,  $Z_{in}$  the characteristic impedance of absorber, and  $Z_o$  the characteristic impedance of free space.

### 3. RESULTS AND DISCUSSION

M-type Ba-hexaferrite has been considered to study the effect of particle size. Thermal study using DSC has been carried out to decide annealing temperature.

#### 3.1. Thermal Analysis

Thermal analysis of the 'as-synthesized' hexaferrite powder ( $P_0$ ) shows two exothermic peaks as shown in Fig. 1, which correspond to two TG steps with an overall weight loss of 17% in the range of 25°–800°C, after which no weight loss was noticed. The first exothermic peak was observed at 338°C, which is sharp and intense, that corresponds to the decomposition of un-reactive organic material induced by excess citric acid. However, this excess citric acid decomposes to CO, CO<sub>2</sub>, organic products and water vapor during heat treatment and helps in reducing the particle size by inhibiting the particle growth [14]. Decomposition is a very complex process which involves removal of water and excess nitrates, decomposition of anhydrous citrate complex and free citric acid through intermediate phases. The nature of decomposition processes is very sensitive to the gel structure and

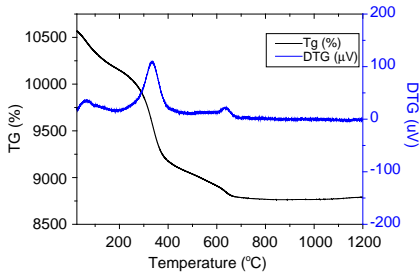


**Figure 1.** DTG-TG traces of as-synthesised Ba-hexaferrite ( $P_0$ ).

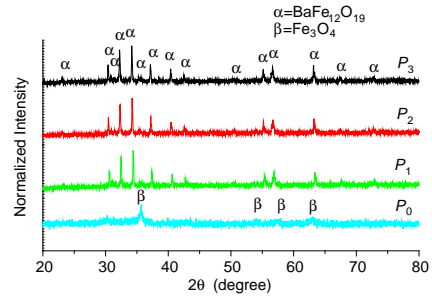


**Figure 2.** Indexed XRD patterns of ferrite samples  $P_0$ ,  $P_1$ ,  $P_2$  and  $P_3$ .

heating rate. The second exothermic peak was observed at  $637^\circ\text{C}$  that indicates the transformation of amorphous phase to the crystalline phase of hexaferrite, which corresponds to the formation of pure  $\text{BaFe}_{12}\text{O}_{19}$  phases. Above  $800^\circ\text{C}$ , the TG curve becomes smoother, suggesting the completion of reaction, i.e., the complete formation of crystalline Ba M-type hexaferrite. It has been observed from the literature [15–17] that with the increase in annealing temperature from ‘as-synthesized’ condition, both complex permittivity and permeability increase. Therefore, a high annealing temperature, i.e.,  $1100^\circ\text{C}$  was selected for heat treatment and particles of different size were obtained by annealing ‘as-synthesized’ sample for different holding times.

### 3.2. XRD Analysis

The indexed XRD patterns of the samples  $P_0$ ,  $P_1$ ,  $P_2$  and  $P_3$  are shown in Fig. 2. It can be inferred from the results that the ferrite powder  $P_0$  shows only the peak corresponding to  $\text{Fe}_3\text{O}_4$ ,  $2\theta = 35.707^\circ$  (ICSD collection code: 158746). When annealed at  $1100^\circ\text{C}$  for different holding times ( $P_1$ ,  $P_2$  and  $P_3$ ), the single phase corresponding to  $\text{BaFe}_{12}\text{O}_{19}$ ,  $2\theta = 34.268^\circ$  (ICSD collection code: 60986) has been observed. Reproducibility of phase formation was checked by numerous reactions. As expected, the crystallite size increases with the increasing annealing time from 2 to 8 hours. The lattice parameters of the unit cell obtained by nonlinear least-squares refinement of XRD data using UnitCell Program CCP14 [18] that gives lattice parameters ‘ $a$ ’ and ‘ $c$ ’ of samples  $P_0$ ,  $P_1$ ,  $P_2$  and  $P_3$  which is shown in Table 1. XRD analysis reveals that lattice parameters and crystallite size increases with the increasing annealing time. Similar trend is also reported by Meza et al. [19]. This may be explained as more oxygen atoms are

absorbed by the hexaferrite structure with the increasing annealing time. These oxygen atoms seem to be absorbed in the  $c$ -direction as the  $c/a$  ratio increases with time (Table 1) and correspondingly the volume of the unit cell also increases. This can also be explained as the intensity of the peak of annealed samples corresponding to  $2\theta = 35.697^\circ$  increases with increasing time meaning more dissociation of oxygen atom of  $\text{Fe}_3\text{O}_4$  into the crystal structure of hexaferrite.

### 3.3. FE-SEM and TEM Analysis

The FE-SEM and TEM micrographs of synthesized ferrite samples  $P_0$ ,  $P_1$ ,  $P_2$  and  $P_3$  are shown in Figs. 3 and 4 respectively and corresponding particle sizes are listed in Table 1. The particles seem to have spherical shaped morphology with an average particle size of 37 nm for sample  $P_0$  (Figs. 3(a) and 4(a)). As the 'as-synthesized' ferrite powder  $P_0$  was annealed at  $1100^\circ\text{C}$ , the small, amorphous and spherical shaped

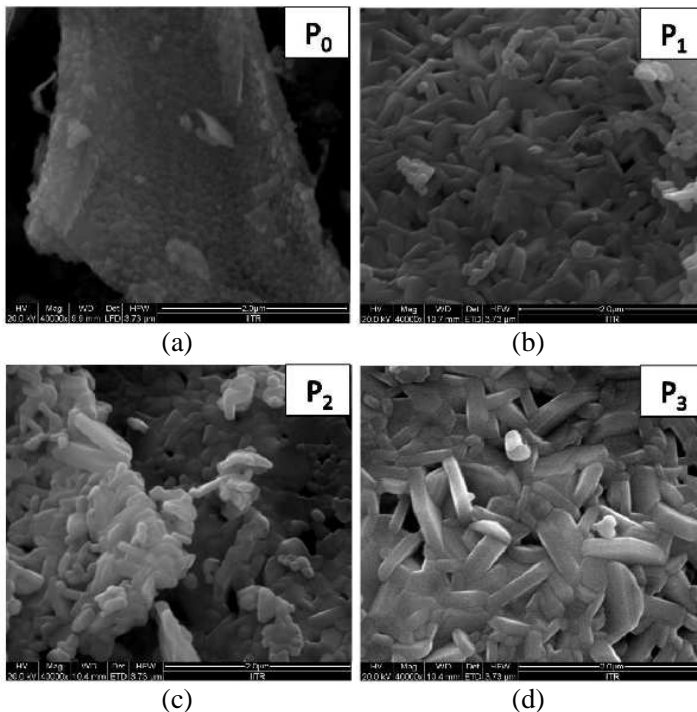


**Figure 3.** FESEM micrographs of ferrite powder samples, (a)  $P_0$ , (b)  $P_1$ , (c)  $P_2$ , and (d)  $P_3$ .

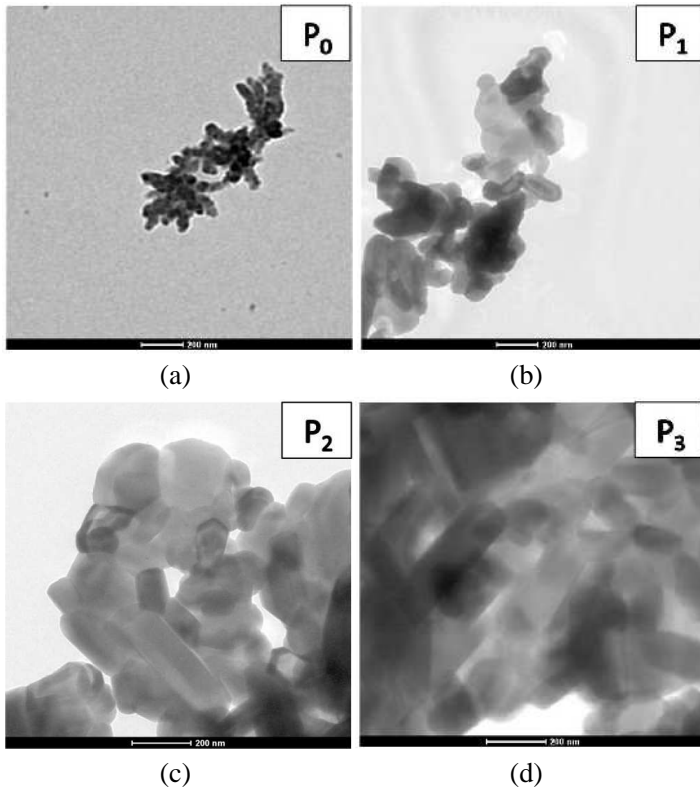


**Figure 4.** TEM micrographs of ferrite powder samples, (a)  $P_0$ , (b)  $P_1$ , (c)  $P_2$ , and (d)  $P_3$ .

particles crystallize to form single phase hexagonal platelets and the particles grow in size (Figs. 3(b)–(d) and 4(b)–(d)). These materials with hexagonal platelet morphologies are potential materials for the RADAR absorption applications [20]. The quantitative metallographic approach was used to determine average particle size of the ferrite samples  $P_0$ ,  $P_1$ ,  $P_2$  and  $P_3$  using FESEM and TEM images. Both the average particle size and standard deviation were found to increase with the increase in annealing time. Most of the particles are of same morphology with an average particle size of 125 nm and standard deviation of 70 nm for the ferrite sample  $P_1$  (Figs. 3(b) and 4(b)). With the increased annealing time for ferrite sample  $P_2$ , smaller particles start diffusing into bigger particles and therefore, particles of bigger size are found (Figs. 3(c) and 4(c)) with the average particle size of 156 nm and standard deviation of 108 nm. Sample was again annealed

for longer time, i.e., 8 hours (ferrite sample  $P_3$ ) as shown in Figs. 3(d) and 4(d), nearly all small particles disappear and grow to a size of 240 nm (average value) with standard deviation of 134 nm, which can be explained by Ostwald ripening [21].

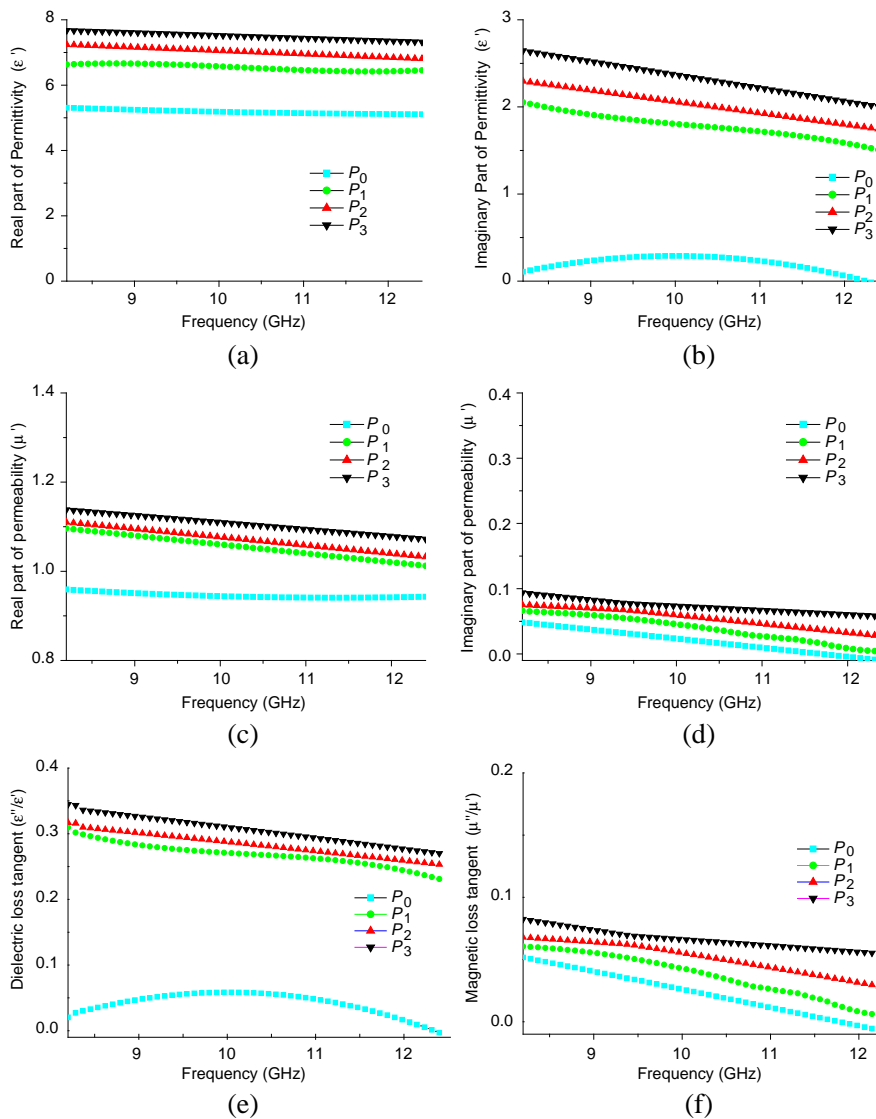


**Figure 5.** Frequency dependent complex dielectric properties of BaFe<sub>12</sub>O<sub>19</sub> ferrite.

### 3.4. Dielectric Constant Measurement

Complex permittivity and permeability values of materials are the representation of the dielectric and magnetic properties of the materials. The real parts ( $\epsilon'$ ,  $\mu'$ ) of complex permittivity and permeability represent the storage capability of electric and magnetic energy. The imaginary parts ( $\epsilon''$ ,  $\mu''$ ) represent the loss of electric and magnetic energy [12]. The real and imaginary parts of complex permittivity (Figs. 5(a) and (b)) and permeability (Figs. 5(c) and (d)) of BaFe<sub>12</sub>O<sub>19</sub> ferrite-epoxy composites are plotted as a function of frequency in X-band (8.2–12.4 GHz) and are in accordance with the reported elsewhere [22]. It has been observed that the complex dielectric constants are decreasing with increasing frequency for all samples annealed at 1100°C that shows a normal dielectric behavior of magnetoplumbite structure. Similar trend has been observed by several other researchers [5, 23, 24]. Both permittivity and permeability values improve after annealing as shown in Figs. 5(a)–(d). The real part of permittivity increased from 5.18 (average value) for sample  $P_0$  to 7.50 (average value) for sample  $P_3$  (Fig. 5(a)). Similar trend has been observed for the imaginary part of permittivity, which increases from an average value of 0.20 for sample  $P_0$  to an average value of 2.33 for sample  $P_3$  (Fig. 5(b)). The real part of permeability increases from 0.95 (average value) for sample  $P_0$  to 1.11 (average value) for sample  $P_3$  (Fig. 5(c)). Similarly, a marginal increase in imaginary permeability is noticed from an average value 0.02 to 0.07 from sample  $P_0$  to  $P_3$  (Fig. 5(d)). Higher values of imaginary components of complex permittivity and permeability are required for a good microwave absorber and are represented by loss tangents [5, 20]. Figs. 5(e) and (f) show frequency dependent dielectric and magnetic loss tangents in the frequency range of 8.2–12.4 GHz for all samples. The dielectric loss tangent for BaFe<sub>12</sub>O<sub>19</sub> ferrite increases with the increase in the average particle size from an average value of 0.04 for  $P_0$  sample to 0.31 (average value) for sample  $P_3$ . With the increase in average particle size, the loss tangent value continuously increases. Similar trend has been observed for the magnetic loss tangent (an increase in the average value of 0.02 for sample  $P_0$  to 0.07 for sample  $P_3$ ). The increase in complex permittivity and permeability is attributed to the change in the lattice parameters and the particle size.

### 3.5. Reflection Loss Study

The variation in reflection loss (RL) with frequency for all samples of BaFe<sub>12</sub>O<sub>19</sub> ferrite-epoxy composite of 2.8 mm thickness in the frequency range of 8.2–12.4 GHz is shown in Fig. 6. The RL for sample

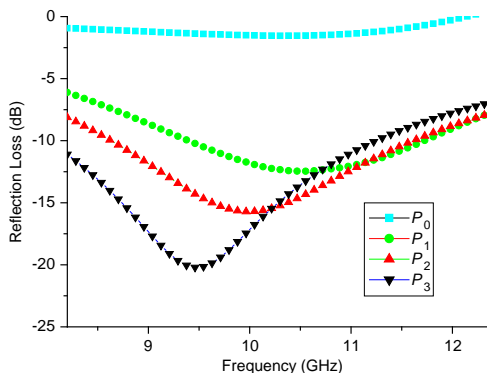


**Figure 6.** The effect of HT time on reflection loss of BaFe<sub>12</sub>O<sub>19</sub> ferrite for  $t = 2.8$  mm thickness.

$P_0$  is low for all the frequencies with a minimum value of RL  $-2.33$  dB at 10.384 GHz. The RL is evidently improved to a minimum value of  $-12.46$  dB at 10.55 GHz for  $P_1$  with a bandwidth of 2.18 GHz, where the bandwidth is defined as the frequency width, in which the reflection loss is less than  $-10$  dB (corresponding to 90% absorption) [25]. The values of minimum reflection losses are  $-15.71$  dB for  $P_2$  at 9.96 GHz and  $-20.21$  for  $P_3$  at 9.46 GHz and  $-10$  dB bandwidths are 2.86 and 3.02 GHz respectively. The minimum RL and bandwidth increases with the average particle size from  $P_1$  to  $P_3$ . Such wide absorption widths and high absorption loss peaks indicate that it has wide application as microwave absorbing material. This may be due to the reason that the inhomogeneous growth of particles creates the suitable size of network's holes as reported by Zhou et al. [26] where the author has described about these network's holes created due to increase in the aspect ratio. The larger the standard deviation, the larger will be the size of pores in the composite, which leads to more internal reflection and as a result less direct reflection on the surface of the material. But it will reduce the related effect of microwave absorption if standard deviation becomes too large.

#### 4. CONCLUSIONS

Single phase M-type Ba-hexaferrite (BaFe<sub>12</sub>O<sub>19</sub>) powder of different particle sizes was synthesized by sol-gel autocombustion method. The average particle size, which plays an important role in electronic properties of materials, increases with the increase in annealing time. The complex dielectric properties, loss tangents, reflection loss

and bandwidth increase with the increase in average particle size (i.e., annealing time). The minimum reflection loss of  $-20.21$  dB (corresponding to 99% power attenuation) at 9.46 GHz was obtained for average particle size of 240 nm. It is observed that particle size may play a major role while controlling the absorption characteristics at microwave frequencies which may reduce the complexity of doping different elements.

## ACKNOWLEDGMENT

The authors acknowledge the All India Council for Technical Education (AICTE), Govt. of India for the fellowship granted to the first author of this study.

## REFERENCES

1. Vinoy, K. J. and R. M. Jha, "Trends in radar absorbing materials technology," *Sadhana*, Vol. 20, 815–850, 1995.
2. Singh, P., V. K. Babbar, A. Razdan, S. L. Srivastava, V. K. Agrawal, and T. C. Goel, "Dielectric constant, magnetic permeability and microwave absorption studies of hot-pressed Ba-CoTi hexaferrite composites in X-band," *Journal of Material Science*, Vol. 41, 7190–7196, 2006.
3. Mu, G., N. Chen, X. Pan, H. Shen, and M. Gu, "Preparation and microwave absorption properties of Barium ferrite nanorods," *Materials Letters*, Vol. 62, 840–842, 2008.
4. Ohlan, A., K. Singh, N. Gandhi, A. Chandra, and S. K. Dhawan, "Microwave absorption properties of NiCoFe<sub>2</sub>O<sub>4</sub>-graphite embedded poly (o-phenetidine) nanocomposites," *AIP Advances*, Vol. 1, 032157, 2011.
5. Ozgiir, U., Y. Alivov, and H. Morkoc, "Microwave ferrites, part 1: Fundamental properties," *Journal of Material Science: Materials Electronics*, Vol. 20, 789–834, 2009.
6. Hlavacek, V. and J. A. Puszynski, "Chemical engineering aspects of advanced ceramic materials," *Industrial & Engineering Chemistry Research*, Vol. 35, 349–377, 1996.
7. Liu, M., X. Shen, F. Song, J. Xiang, and R. Liu, "Effect of heat treatment on particle growth and magnetic properties of electrospun Sr<sub>0.8</sub>La<sub>0.2</sub>Zn<sub>0.2</sub>Fe<sub>11.8</sub>O<sub>19</sub> nanofibers," *Journal of Sol-Gel Science and Technology*, Vol. 59, 553–560, 2011.
8. Bezerra, C. W. B., L. Zhang, H. Liu, K. Lee, A. L. B. Marques, E. P. Marques, H. Wang, and J. Zhang, "A review of heat-

- treatment effects on activity and stability of PEM fuel cell catalysts for oxygen reduction reaction,” *Journal of Power Sources*, Vol. 173, 891–908, 2007.
9. Meshram, M., N. K. Agrawal, B. Sinha, and P. S. Misra, “Characterization of (Co-Mn-Ti) substituted M-type Barium hexagonal ferrite based microwave absorber at X-band,” *IEEE Proceedings of 6th International Symposium on Antennas, Propagation and EM Theory*, 746–749, 2003.
  10. Tang, X., Y. Yang, and K. Hu, “Structure and electromagnetic behavior of  $\text{BaFe}_{12-2x}(\text{Ni}_{0.8}\text{Ti}_{0.7})_x\text{O}_{19-0.8x}$  in the 2–12 GHz frequency range,” *Journal of Alloys and Compounds*, Vol. 477, 488–492, 2009.
  11. Kumar, A., V. Agarwala, and D. Singh, “Effect of Mg-substitution on microwave absorption of  $\text{BaFe}_{12}\text{O}_{19}$ ,” *Advanced Materials Research*, Vol. 585, 62–66, 2012.
  12. Qiu, J., M. Gu, and H. Shen, “Microwave absorption properties of Al- and Cr-substituted M-type barium hexaferrite,” *Journal of Magnetism and Magnetic Materials*, Vol. 295, 263–268, 2005.
  13. Qiu, J., Y. Wang, and M. Gu, “Effect of Cr substitution on microwave absorption of  $\text{BaFe}_{12}\text{O}_{19}$ ,” *Materials Letter*, Vol. 60, 2728–2732, 2006.
  14. Panda, R. N., J. C. Shih, and T. S. Chin, “Magnetic properties of nano-crystalline Gd- or Pr-substituted  $\text{CoFe}_2\text{O}_4$  synthesized by the citrate precursor technique,” *Journal of Magnetism and Magnetic Materials*, Vol. 257, 79–86, 2003.
  15. Tyagi, S., H. B. Baskey, R. C. Agarwala, V. Agarwala, and T. C. Shami, “Development of hard/soft ferrite nanocomposite for enhanced microwave absorption,” *Ceramics International*, Vol. 37, 2631–2641, 2011.
  16. Tyagi, S., H. B. Baskey, R. C. Agarwala, V. Agarwala, and T. C. Shami, “Reaction kinetic, magnetic and microwave absorption studies of  $\text{SrFe}_{12}\text{O}_{19}/\text{CoFe}_2\text{O}_4$  ferrite nanocrystals,” *Transactions of the Indian Institute of Metals*, Vol. 64, 271–277, 2011.
  17. Zhang, H., M. Wu, X. Yao, and L. Zhang, “Complex permittivity, permeability, and microwave absorption of Barium ferrite by citrate sol-gel process,” *Rare Metals*, Vol. 22, 125–130, 2003.
  18. Holland, T. J. B. and S. A. T. Redfern, “Unit cell refinement from powder diffraction data: The use of regression diagnostics,” *Mineralogical Magazine*, Vol. 61, 65–67, 1997.
  19. Meza, V. A., X. Gratens, and R. F. Jardim, “Preparation

- and general physical properties of polycrystalline  $\text{PrBa}_2\text{Cu}_3\text{O}_{7-y}$  obtained from sol-gel precursors,” *Brazilian Journal of Physics*, Vol. 32, 731–738, 2002.
20. Sharma, R., R. C. Agarwala, and V. Agarwala, “Development of radar absorbing nano crystals by microwave irradiation,” *Materials Letters*, Vol. 62, 2233–2236, 2008.
  21. Taylor, P., “Ostwald ripening in emulsions,” *Advances in Colloid and Interface Science*, Vol. 75, 107–163, 1998.
  22. Bahadoor, A., Y. Wang, and M. N. Afsar, “Complex permittivity and permeability of barium and strontium ferrite powders in X, Ku, and K-band frequency ranges,” *Journal of Applied Physics*, Vol. 97, 10F105-1–10F105-3, 2005.
  23. Giannakopoulou, T., L. Kompotiatis, A. Kontogeorgakos, and G. Kordas, “Microwave behavior of ferrites prepared via sol-gel method,” *Journal of Magnetism and Magnetic Materials*, Vol. 246, 360–365, 2002.
  24. Zhang, H., Z. Liu, C. Ma, Y. Xi, L. Zhang, and M. Wu, “Complex permittivity, permeability, and microwave absorption of Zn- and Ti-substituted barium ferrite by citrate sol-gel process,” *Materials Science and Engineering B*, Vol. 96, 289–295, 2002.
  25. Zou, H., S. Li, L. Zhang, S. Yan, H. Wu, S. Zhang, and M. Tian, “Determining factors for high performance silicone rubber microwave absorbing materials,” *Journal of Magnetism and Magnetic Materials*, Vol. 323, 1643–1651, 2011.
  26. Zhou, Z., L. Chu, and S. Hu, “Microwave absorption behaviors of tetra-needle-like ZnO whiskers,” *Materials Science and Engineering B*, Vol. 126, 93–96, 2006.